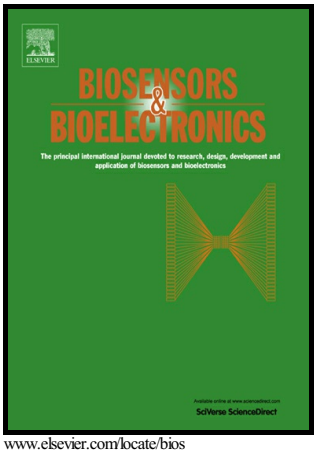

www.elsevier.com/locate/bios

Potential-resolved Faraday cage-type electrochemiluminescence biosensor for simultaneous determination of miRNAs using functionalized g-C_3N_4 and metal organic framework nanosheets

Huili Shao, Han Lin, Jing Lu, Yufang Hu, Sui Wang, Youju Huang, Zhiyong Guo

PII: S0956-5663(18)30575-X
DOI: https://doi.org/10.1016/j.bios.2018.07.064
Reference: BIOS10653

To appear in: *Biosensors and Bioelectronic*

Received date: 11 May 2018
Revised date: 16 July 2018
Accepted date: 30 July 2018

Cite this article as: Huili Shao, Han Lin, Jing Lu, Yufang Hu, Sui Wang, Youju Huang and Zhiyong Guo, Potential-resolved Faraday cage-type electrochemiluminescence biosensor for simultaneous determination of miRNAs using functionalized g-C_3N_4 and metal organic framework nanosheets, *Biosensors and Bioelectronic,* https://doi.org/10.1016/j.bios.2018.07.064

Potential-resolved Faraday cage-type electrochemiluminescence biosensor for simultaneous determination of miRNAs using functionalized g-C_3N_4 and metal organic framework nanosheets

Huili Shao[a], Han Lin[a], Jing Lu[a], Yufang Hu[a], Sui Wang[a], Youju Huang[b,c*], Zhiyong Guo[a*]

[a]*School of Materials Science and Chemical Engineering, The State Key Laboratory Base of Novel Functional Materials and Preparation Science, Ningbo University, Ningbo 315211, P. R. China*

[b]*Key Laboratory of Marine Materials and Related Technologies, Zhejiang Key Laboratory of Marine Materials and Protective Technologies, Division of Polymer and Composite Materials, Ningbo Institute of Materials Technology & Engineering, Chinese Academy of Sciences, Ningbo 315201, P. R. China*

[c]*Max Planck Institute for Polymer Research, Ackermannweg 10, 55128, Mainz, Germany*

guozhiyong@nbu.edu.cn
huangyouju@mpip-mainz.mpg.de

[*]Corresponding author.

ABSTRACT

Here, a novel Faraday cage-type electrochemiluminescence (ECL) biosensor was

presented for simultaneous determination of miRNA-141 and miRNA-21 based on the potential-resolved strategy. In this work, capture units were prepared by immobilizing hairpin DNA1 (HP1) and hairpin DNA2 (HP2) on Fe_3O_4@Au nanocomposites, while g-C_3N_4@AuNPs nanocomposites labelled by signal DNA1 (sDNA1) and ruthenium-based metal organic framework (Ru-MOF) nanosheets labelled by signal DNA2 (sDNA2) were used as signal units. In this proposed biosensor, signal units g-C_3N_4@AuNPs-sDNA1 and Ru-MOF-sDNA2 could exhibit two strong and stable ECL emissions at −1.4 V and +1.5 V respectively, which could be used as effective potential-resolved signal tags. Moreover, taking advantage of the proposed Faraday cage-type model, all electrochemiluminophores in the signal units could take part in electrode reactions, the signal units became part of the electrode surface and extended the outer Helmholtz plane (OHP) of the proposed electrode, and then the detection sensitivity was improved greatly. Accordingly, dual targets miRNA-141 and miRNA-21 could be detected within the linear range of 1 fM to 10 pM, with the detection limit of 0.3 fM. Meanwhile, the proposed miRNA assay exhibited high selectivity and sensitivity, even for practical analysis in human serum. So, this potential-resolved ECL biosensor is proved to be a feasible tool for dual targets detection of miRNAs in clinical diagnosis.

Keywords: Potential-resolved; Dual targets; Ultrasensitive miRNA detection; Faraday cage-type; Electrochemiluminescence biosensor

Introduction

MicroRNAs (miRNAs), a class of endogenous noncodesmall molecules (18–22nt) [Dong et al., 2012], play important roles as post-transcriptionalregulators for gene expression in a broad range of animals, plants, and viruses [Ambros et al., 2004; Esquela-Kerscher et al., 2006; Lee et al., 1993]. It is associated with a wide range of biological processes, such as cell proliferation, apoptosis and death [Sawyers et al., 2008]. Research evidence has shown that aberrant (up- or down-regulated) expression of miRNAs is closely related to the occurrence of various diseases, especially human cancers, neurological diseases, viral infections and diabetes [Ryoo et al., 2013]. And accumulated evidence has demonstrated that miRNA is a potential class of biomarker candidate for cancer classification [Lu et al., 2005], early disease diagnosis [Calin et al., 2006], and prognosis [Cissell et al., 2007]. But, the relationship between miRNAs and diseases is generally not simple one-to-one. Using only one single miRNA as a biomarker may induce false positive results for clinical diagnosis due to insufficient information, which may cause anxiety for the individuals and lead to unnecessary biopsies or surgery [Kong et al., 2012; Ohtsuka et al., 2015]. In fact, a disease is sometimes expressed simultaneously by several miRNAs. For example, the levels of miRNA-141 and miRNA-21 are simultaneously elevated in the case of prostate cancer [Foj et al., 2017; Pan et al., 2010; Agaoglu et al., 2011; Jou et al., 2017]. It suggests that multiplexed biomarkers assay could not only enhance the accuracy of cancer diagnostics but also offer several potential advantages, in terms of improved detection efficiency, simplified analytical procedures, and reduced cost.

Currently, a wide variety of analytical methods and biosensors have been adopted for multianalyte determination. Common approaches utilized for multianalyte of miRNAs include fluorescence [Jie et al., 2017], chemiluminescent [Yue et al., 2017], electrochemical [Zhou et al., 2017; Yang et al., 2014], Raman [Yuan et al., 2017] and electrochemiluminescence (ECL) [Peng et al., 2017]. Among these methods, ECL does not need light source, resulting in low background, high detection sensitivity and simple instrumentation [Gao et al., 2016; Shi et al., 2016]. Moreover, since the luminescence emission from the ECL probe is controlled by potential, it is feasible to develop a potential-resolved ECL method that could detect multiply analytes in a potential scanning cycle. And, the potential-resolved strategy is not related with the spectrum difference of probes, thus, no beam splitter or filter is needed to distinguish signals.

With the development of nanotechnology, many nanomaterials have been used in ECL field to improve analytical performance. Among these nanomaterials, graphitic-phase carbon nitride nanosheet (g-C_3N_4), an unique and new type of graphene-like carbon-based nanomaterial with high water-dispersibility and good biocompatibility, has recently been proved to be an effective, strong, and stable ECL emitter [Kroke et al., 2004; Cui et al., 2000; Bojdys et al., 2008; Cheng et al., 2013]. This layered material has been used in ECL sensors for sensitive determination of carcinoembryonic antigen (CEA) [Chen et al., 2014], DNA [He et al., 2015] and miRNA [Feng et al., 2016]. Meanwhile, 2D metal-organic framework (MOF) nanosheets, as a new type of porous material, also present many excellent

properties such as novel structure, large specific surface area and high conductivity. They also possess high level of structural tailor properties, which can be easily used to load plenty of antibodies, enzymes, DNAs and various labels [Wang et al., 2011; Kent et al., 2012; Carne et al., 2011; Rocca et al., 2011]. Profiting from these excellent properties, we proposed a new concept of Faraday cage-type model based on multi-functionalized 2D nanomaterials by extending the outer Helmholtz plane (OHP) of the proposed ECL biosensor, which can overcome the low electrode reaction efficiency [Guo et al., 2016; Guo et al., 2016; Wu et al., 2016]. Briefly, in a Faraday cage-type ECL biosensor, the multi-functionalized 2D nanomaterials in the signal unit could lap on the surface of an electrode, as if the signal unit is immobilized directly on the surface of the electrode or even "in the electrode", making all the electrochemiluminophores in the signal unit are electroactive and able to produce ECL signals. In other words, 2D nanomaterials used in the signal unit extend the effective OHP region, favor the electron transfer on the electrode interface, increase the number of effective electrochemiluminophores, and thus then enhance the ECL intensity of the proposed biosensor greatly. However, up to now, there has been no report using two 2D nanomaterials for a potential-resolved ECL system to detect dual miRNAs simultaneously.

Herein, inspired by the 2D nanomaterials g-C_3N_4@AuNPs and Ru-MOF that could exhibit two strong and stable ECL emissions at different potentials, we prepared two signal units of g-C_3N_4@AuNPs-sDNA1 and Ru-MOF-sDNA2 to implement dual targets detection. Based on them, a novel potential-resolved Faraday cage-type ECL

biosensor was designed and constructed for the simultaneous detection of miRNA-141 and miRNA-21, which could provide a promising alternative for multiple-target analysis in clinical diagnosis.

2. Experimental

2.1. Reagents and materials

Tris(2-carboxyethyl) phosphine hydrochloride (TCEP), 6-mercapto-1-hexanol (MCH), 1-ethyl-3-(3-dimethylaminopropyl) carbodiimide hydrochloride (EDC) and N-hydroxysuccinimide (NHS) were purchased from Sigma-Aldrich (St. Louis, MO, USA). Tris(4,4'-dicarboxylicacid-2,2'-bipyridyl)ruthenium (II) dichloride ($[Ru(dcbpy)_3]^{2+}$) was purchased from Suna Tech Inc. (Suzhou, China). Potassium persulfate ($K_2S_2O_8$), tripropylamine (TPrA), zinc nitrate ($Zn(NO_3)_2$), n-propanol (NPA), ethylenediamine tetraacetic acid (EDTA), hydrogen tetrachloroaurate (III) hydrate ($HAuCl_4 \cdot 4H_2O$) and sodium citrate were purchased from Sinopharm Chemical Reagent Co., Ltd. (Shanghai, China). Diethy pyrocarbonate (DEPC) was purchased from Sangon Biotech (Shanghai, China). All DNA and miRNA sequences used in this study were synthesized by Sangon Biotech (Shanghai, China) and the sequences are listed in Table S1. The buffer and detection solution used in this study are depicted in Supplementary material.

2.2. Apparatus

UV-visible spectra were obtained with a UV-1800 spectrophotometer (Shimadzu,

Japan). Zeta potential analysis was acquired using a Malvern Zana ZS 90 Mastersizer (Malvern, UK). X-ray diffraction (XRD) characterization was performed using X-ray powder diffractometer (Bruker, D8 Focus, Karlsruhe, Germany) with Cu Ka radiation at room temperature. Morphologies of different nanocomposites were characterized by scanning electron microscopy (SEM, Hitachi SU-70, Tokyo, Japan) at an accelerating voltage of 15-20 kV and transmission electron microscopy (TEM, JEM-2100, Electronic Co., Ltd., Japan) at an accelerating voltage of 200 kV. Electrochemical experiments including cyclic voltammetry (CV) and electrochemical impedance spectroscopy (EIS) were performed on a CHI 660E electrochemical workstation (Shanghai CH Instruments, China), and ECL measurements were performed with a custom-built ECL detection equipment that mainly contains a BPCL ultra-weak chemiluminescence analyzer (Institute of Biophysics, Chinese Academy of Sciences, Beijing, China) and CHI 1100A electrochemical workstation (Chenhua Instrument Company, Shanghai, China). A conventional three-electrode system, which consists of a magnetic glass carbon electrode (MGCE, 3 mm diameter, Wuhan, China) as working electrode, an Ag/AgCl (3 M KCl) electrode as reference electrode and a platinum coil as counter electrode, was used.

2.3. Synthesis of materials

2.3.1. Synthesis of signal unit 1 (g-C_3N_4@AuNPs-sDNA1)

Signal unit 1 (g-C_3N_4@AuNPs-sDNA1) was prepared through mixing g-C_3N_4@AuNPs (see the Supplementary material) [Lin et al., 2014] and sDNA1. As shown in Scheme 1A, firstly, 200 μL of as prepared g-C_3N_4@AuNPs solution was

mixed with 100 μL of 2 μM sDNA1 in 0.1 M PBS, followed by shaking for 4 h. Then, the compounds were centrifuged at 5000 rpm for 15 min to remove free sDNA1 and washed with water. Subsequently, 100 μL of 2 mM MCH was added and allowed to react for 1 h to block non-specific binding sites and force the modified DNA probe to adopt an upright surface orientation that would favor further hybridization. After the composites were washed and reconstructed in 100 μL of DNA hybridization buffer, the signal unit 1 was finally obtained.

2.3.2. Synthesis of signal unit 2 (Ru-MOF-sDNA2)

The preparation procedure of signal unit 2 Ru-MOF-sDNA2 composite is shown in Scheme 1B. Firstly, 200 μL of as-prepared Ru-MOF nanosheets (see the Supplementary material) [Zhang et al., 2015] was added into 200 μL of a mixture solution containing 100 mg/mL EDC and 10 mg/mL NHS. After adjusting pH to 5.0, the solution was shaken for 1 h in order to activate the carboxyl groups of Ru-MOF, and then the resulted composite was thoroughly washed by water. Subsequently, 100 μL of 2 μM sDNA2 was added and shaken for another 4 h. Finally, signal unit 2 Ru-MOF-sDNA2 was obtained after washing and reconstituting in 100 μL of DNA hybridization buffer.

2.3.3. Synthesis of capture units (Fe_3O_4@AuNPs-HP1 and Fe_3O_4@AuNPs-HP2)

Firstly, hairpin DNA1 and hairpin DNA2 were activated with 10 mM TCEP at 4 °C for 1 h. Then, 100 μL of Fe_3O_4@AuNPs (see the Supplementary material) [Liu et al., 2014] and 50 μL of 2 μM hairpin DNA1 were mixed, and then incubated at 37 °C in constant temperature oscillator for 16 h. Afterwards, the compounds were separated

by magnet to remove free hairpin DNA and washed with water. Then, 50 μL of 2 mM MCH solution was added and incubated for 1 h. Finally, after being washed and dispersed in 100 μL of DNA hybridization buffer, capture unit Fe_3O_4@AuNPs-HP1 was obtained and stored at 4 °C. Meanwhile, capture unit Fe_3O_4@AuNPs-HP2 was prepared the same as above except that hairpin DNA1 was replaced by hairpin DNA2.

2.4. Fabrication of the potential-resolved dual targets ECL biosensor

To obtain a mirror-like surface, the bare MGCE was polished carefully with 1.0, 0.3 and 0.05 μm alumina respectively and washed ultrasonically with water and ethanol for 5 min. After drying at room temperature, 10 μL of capture units Fe_3O_4@AuNPs-HP1 and Fe_3O_4@AuNPs-HP2 was coated onto MGCE. After drying in air for a few minutes, the electrode was incubated in miRNA-141 and miRNA-21 mixture solution for 2 h at 37 °C to capture the targets. Finally, the ECL biosensor was fabricated completely by incubating the electrode with 10 μL of signal unit 1 and signal unit 2 for 2 h at 37 °C. After washing with buffer to remove the physically adsorbed signal units, the Faraday cage-type ECL biosensor was obtained and stored at 4 °C when not in use.

2.5. ECL detection

The fabricated dual targets Faraday cage-type ECL biosensor was immersed in 0.1 M PBS (pH 7.4) containing 20 mM $K_2S_2O_8$ and 60 mM TPrA, and potential scanned from −1.4 to +1.5 V with a scan rate of 100 mV/s. The ECL signals were recorded with the voltage of the photomultiplier at 800 V.

3. Results and discussion

3.1. Characterization of different nanomaterials

The morphologies and size of different nanocomposites were monitored by using TEM techniques. Figure 1A displays that g-C_3N_4 has a two-dimensional sheet-like structure. As to g-C_3N_4@AuNPs (Figure 1B), a large number of AuNPs were uniformly distributed on the g-C_3N_4 surface without any agglomeration, due to the fact that g-C_3N_4 was positively charged while AuNPs were negatively charged. As can be seen from Figure S1, Zeta potential of g-C_3N_4 was +44.0 mV and that of AuNPs was −26.3 mV. Therefore, g-C_3N_4@AuNPs could be easily synthesized based on the electrostatic absorption forces between AuNPs and g-C_3N_4. And, a band of g-C_3N_4@AuNPs at 525 nm in UV-vis absorption spectra (Figure S2) near the characteristic absorption peak of spherical AuNPs was observed, demonstrating its correct formation.

Ru-MOF exhibits a good two-dimensional sheet-like structure (Figure 1C), too. Meanwhile, XRD data in Figure S3 indicates that main diffraction peaks of luminescence-functionalized Ru-MOF nanosheets prepared are in agreement with the previous literature [Xiong et al., 2015]. As to Fe_3O_4@AuNPs, they were uniformed monodisperse nanospheres, formed by a Fe_3O_4 nanosphere with a diameter of about 80-100 nm and coated by numerous individual AuNPs with a diameter of about 5-15 nm (Figure 1D). In addition, SEM and EDS results (Figure S4) show that the

elemental compositions of Fe_3O_4@AuNPs were Fe, C, O and Au. All above results suggested the successful preparation of Fe_3O_4@AuNPs.

3.2. Characterization of the potential-resolved Faraday cage-type ECL biosensor

The fabrication process of potential-resolved Faraday cage-type ECL biosensor for detection of dual miRNAs is illustrated in Scheme 1. Initially, capture units Fe_3O_4@AuNPs-HP1 and Fe_3O_4@AuNPs-HP2 were coated onto MGCE. When miRNA-141 (target 1) and miRNA-21 (target 2) were present, they would respectively hybridize with HP1 and HP2 in capture units, open the stem-loop structure of HP1 and HP2 through the tension force of DNA double chain. Then, the tail ends of HP1 and HP2 were exposed, which were complementary to signal DNA1 and signal DNA2 respectively, and then hybridized with them. Thus, the signal units were immobilized on the modified electrode by forming the capture unit-targets-signal unit complex. Because g-C_3N_4@AuNPs and Ru-MOF were built on two-dimensional layered nanomaterials and would exhibit two strong and stable ECL emissions at different potentials, the Faraday cage-type ECL biosensor for dual targets miRNA-141 and miRNA-21 was constructed, as illustrated in Figure 1E and Figure 1F. Benefiting from this strategy, all the electrochemiluminophores near the OHP are "effective" in participating in the electrochemical reactions, thus greatly enhancing the ECL signal.

The stepwise fabrication of the biosensor was characterized by CV and EIS using $[Fe(CN)_6]^{3-/4-}$ as electrochemical probe. As shown in Figure 2A and 2B, there was a

pair of well-defined redox peaks on the bare MGCE (curve a in 2A), and the electron transfer resistance R_{et} was small as about 300 Ω (curve a in 2B). After capture units were immobilized, the peak current decreased obviously (curve b in 2A) and R_{et} increased to about 900 Ω (curve b in 2B), due to the fact that the DNA sequences immobilized on capture units hindered the electron transfer on the electrode interface. When miRNA-141 and miRNA-21 hybridized with capture units, the peak current decreased further (curve c in 2A) and R_{et} increased to about 1300 Ω (curve c in 2B). However, after signal unit 1 and signal unit 2 were introduced, the peak current greatly increased (curve d in 2A) and R_{et} decreased to about 600 Ω (curve d in 2B), because g-C_3N_4@AuNPs and Ru-MOF composites had excellent electric conductivity and thus promoted the electron transfer efficiency significantly. It also demonstrated the successful construction of Faraday cage-type ECL biosensor to a certain extent.

CV responses of the prepared biosensor with or without signal units are shown in Figure 2C. There was no redox peak without signal units (solid line). While signal units were immobilized, two redox peaks at about −1.2 V and +1.1 V could be found, corresponding to signal unit 1 g-C_3N_4@AuNPs-sDNA1 and signal unit 2 Ru-MOF-sDNA2 respectively. Additionally, ECL signals were used to characterize the stepwise fabrication of the biosensor too. As shown in Figure 2D, the ECL signal of the bare MGCE was not found (curve a). Even when capture units (curve b), targets miRNA-141 and miRNA-21 were immobilized onto the electrode surface step by step, the ECL intensity was near to zero due to the absence of luminophores. However, after incubating in the mixture solution of signal unit 1 and signal unit 2, two obvious

increments in ECL signals were observed (curve d), demonstrating that the ECL signals originated from electrochemiluminophores g-C_3N_4@AuNPs and Ru-MOF in signal units. Above results suggested that the potential-resolved Faraday cage-type ECL biosensor for simultaneous detection of two miRNAs during one potential scanning was fabricated successfully.

3.3. Detection of miRNA-141 and miRNA-21 using the ECL biosensor

The proposed biosensor was exploited to detect dual targets miRNA-141 and miRNA-21 at a series of concentration under the optimum conditions (see the Supplementary material). As presented in Figure 3A, the ECL intensity increased gradually with increasing concentration of miRNA-141 and miRNA-21, respectively. Both calibration plots exhibited a good linear relationship between the ECL intensity and the logarithm of the analyte concentration from 1 fM to 10 pM of miRNA-141 (Figure 3B) and miRNA-21 (Figure 3C). The linear regression equations were y = 1157.28 + 2076.77*lg$x$ (fM) with a correlation coefficient R = 0.984 for miRNA-141 and y = 1341.92 + 2757.00*lg$x$ (fM) with R = 0.995 for miRNA-21. And, the limit of detection (LOD) for miRNA-141 and miRNA-21 could be roughly estimated as 0.3 fM based on signal/noise = 3, which was more sensitive than those previously reported (Table S2) [Jie et al., 2017; Zhou et al., 2017; Yang et al., 2014; Yuan et al., 2017; Peng et al., 2017]. Above results indicate that the proposed biosensor was capable of detecting miRNA-141 and miRNA-21 simultaneously and possessed low detection limits with wide linear ranges, so it has a potential for practical applications

in early diagnosis.

3.4. Stability, reproducibility and specificity of the ECL biosensor

The stability of the ECL biosensor was examined by consecutive cyclic potential scans for 8 cycles. As depicted in Figure 4A, the ECL intensity shows no obvious change, and the relative standard deviations (RSDs) of miRNA-141 and miRNA-21 were found to be 2.5% and 3.9% respectively. Furthermore, the ECL intensity was 93.8% and 95.2% of the initial value for miRNA-141 and miRNA-21 respectively, after a storage period of 2 weeks at 4 °C. Those results demonstrated the excellent storage stability of the proposed biosensor.

Reproducibility is another significant factor to estimate the performance of the proposed biosensor. Ten replicate measurements of target miRNA-141 and miRNA-21 at 10 fM showed that RSDs were 5.9% and 5.4% respectively, indicating a good reproducibility and precision.

Moreover, the specificity of the designed biosensor was further investigated. The ECL response toward the targets of 10 fM miRNA-141 and miRNA-21 were compared against other three possible interferences, including miRNA-101, miRNA-122 and miRNA-155. As can be seen from Figure 4B, when incubated in 100 pM miRNA-101, miRNA-122 and miRNA-155 respectively, the ECL intensity values are comparable with those of the blank. As to targets miRNA-141 and miRNA-21 individually and their mixture, even the concentration of them was low as 10 fM, the ECL intensity was significant. It indicates that the proposed ECL biosensor exhibited

outstanding specificity as expected.

3.5. Application of the ECL biosensor for serum samples

To evaluate the reliability and practicability of the developed ECL biosensor in clinical analysis, the proposed biosensor was investigated by determining samples spiked with miRNA-141 and miRNA-21 at different concentrations. The samples were prepared by adding standard miRNA-141 and miRNA-21 solution at different concentrations to blank human serum; the results were presented in Table 1. Acceptable recoveries in the range of 93.1 to 108.0% for miRNA-141 and 92.0 to 109.6% for miRNA-21 respectively, and the corresponding RSD ranging from 4.1 to 7.4% for miRNA-141 and 4.3 to 8.7% for miRNA-21 were achieved, indicating that the developed ECL biosensor was an efficient tool for ultrasensitive simultaneous determination of miRNA-141 and miRNA-21 in human serum.

Conclusions

In summary, a novel potential-resolved Faraday cage-type ECL biosensor was fabricated for sensitive detection of two different miRNAs based on functionalized g-C_3N_4 and Ru-MOF nanosheets, which provided two well-separated and sensitive ECL signals at −1.4 V and +1.5 V during one potential scanning. In addition, the detection sensitivity could be improved greatly, due to the employment of the Faraday cage-type strategy. Results indicate that the proposed ECL biosensor had an excellent

detection sensitivity, wide linear range and good accuracy towards real samples. Therefore, this work is a promising approach for potential-resolved ECL detection of dual targets, and it has a great potential in early detection of cancer-related miRNAs with favorable analytical performance.

Acknowledgements

Financial support from the Science and Technology Department of Zhejiang Province of China (2016C33176), the National Natural Science Foundation of China (41576098, 81773483, 21605089) are gratefully acknowledged. This work was also sponsored by K.C. Wong Magna Fund in Ningbo University.

Appendix A. Supplementary material

Supplementary data associated with this article can be found in the online version at http://dx.doi.org/

Additional characterization figures and related results discussions (PDF)

References

Agaoglu, F.Y., Kovancilar, M., Dizdar, Y., Darendeliler, E., Holdenrieder, S., Dalay, N., Gezer, U., 2011. Tumor Biol. 32, 583–588.

Ambros, V., 2004. Nature 431, 350−355.

Bojdys, M.J., Muller, J.O., Antonietti, M., Thomas, A., 2008. Chem. Eur. J. 14, 8177−8184.

Calin, G.A., Croce, C.M., 2006. Nat. Rev. Cancer 6, 857−866.

Carne, A., Carbonell, C., Imaz, I., Maspoch, D., 2011. Chem. Soc. Rev. 40, 291–305.

Chen, L., Zeng, X., Si, P., Chen, Y., Chi, Y., Kim, D.H., Chen G., 2014. Anal. Chem. 86, 4188−4196.

Cheng, C.M., Huang, Y., Wang, J., Zheng, B.Z., Yuan, H.Y., Xiao, D., 2013. Anal. Chem. 85, 2601–2605.

Cissell, K.A., Shrestha, S., Deo, S.K., 2007. Anal. Chem. 79, 4754−4761.

Cui, F.Z., Li, D.J., 2000. Surf. Coat. Technol. 131, 481–487.

Dong, H.F., Jin, S., Ju, H., Hao, K., Xu, L.P., Lu, H., Zhang, X.J., 2012. Anal. Chem. 84, 8670−8674.

Esquela-Kerscher, A., Slack, F.J., 2006. Nat. Rev. Cancer 6, 259−269.

Feng, Q.M., Shen, Z.Y., Li, M.X., Zhang, Z.L., Zhao, W., Xu, J.J., Chen, H.Y., 2016. Anal. Chem. 88, 937−944.

Foj, L., Ferrer, F., Serra, M., Arévalo, A., Gavagnach, M., Giménez, N., Filella, X., 2017. Prostate 77, 573−583.

Gao, W.Y., Liu, Z.Y., Qi, L.M., Lai, J.P., Kitte, S.A., Xu, G.B., 2016. Anal. Chem. 88, 7654–7659.

Guo, Z.Y., Sha, Y.H., Hu, Y.F., Wang, S., 2016. Chem. Commun. 52, 4621−4624.

Guo, Z.Y., Sha, Y.H., Hu, Y.F., Yu, Z.Q., Tao, Y.Y., Wu, Y.J., Zeng, M., Wang, S., Li, X., Zhou, J., Su, X.R., 2016. Anal. Bioanal. Chem. 408, 7203–7211.

He, Y., Li, J.H., Liu, Y., 2015. Anal. Chem. 87, 9777–9785.

Jie, G.F., Zhao, Y., Wang, X.C., Ding, C.F., 2017. Sens. Actuat. B-Chem. 252, 1026−1034.

Jou, A.F.J., Lu, C.H., Ou Y.C., Wang, S.S., Hsu, S.L., Willner, I., Ho, J.A.A., 2015. Chem. Sci. 6, 659−665.

Kent, C.A., Liu, D., Meyer, T.J., Lin, W., 2012. J. Am. Chem. Soc. 134, 3991−3994.

Kong, Y.W., Ferland-McCollough, D., Jackson, T.J., Bushell, M., 2012. Lancet Oncol. 13, E249−E258.

Kroke, E., 2004. Coord. Chem. Rev. 248, 493–532.

Lee, R.C., Feinbaum, R.L., Ambros, V., 1993. Cell 75, 843–854.

Lin, L.S., Cong, Z.X., Li, J., Ke, K.M., Guo, S.S., Yang, H.H., Chen, G.N., 2014. J. Mater. Chem. B 2, 1031−1037.

Liu, M., Wang, Z.Y., Zong, S.F., Chen, H., Zhu, D., Wu, L., Hu, G.H., Cui, Y.P., 2014. ACS Appl. Mater. Interfaces 6, 7371–7379.

Liu, Y., Wei, M., Li, Y., Liu, A., Wei, W., Zhang, Y., Liu, S., 2017. Anal. Chem. 89, 3430–3436.

Lu, J., Getz, G., Miska, E.A., Alvarez-Saavedra, E., Lamb, J., Peck, D., Sweet-Cordero, A., Ebet, B.L., Mak, R.H., Ferrando, A.A., Downing, J.R., Jacks, T., Horvitz, H.R., Golub, T.R., 2005. Nature 435, 834−838.

Manchado, E., Weissmueller, S., Morris, J.P., Chen, C.C., Wullenkord, R., Lujambio, A., Stanchina, E., Poirier, J.T., Gainor, J.F., Corcoran, R.B., Engelman, J.A., Rudin, C.M., Rosen, N., Lowe, S.W., 2016. Nature 534, 647−651.

Ohtsuka, M., Ling, H., Doki, Y., Mori, M., Calin, G.A., 2015. J. Clin. Med. 4, 1651–

1667.

Pan, X., Wang, Z.X., Wang, R., 2010. Cancer Boil. Ther. 10, 1224−1232.

Peng, L., Zhang, P., Chai, Y.Q., Yuan, R., 2017. Anal. Chem. 89, 5036−5042.

Rocca, J.D., Liu, D., Lin, W., 2011. Acc. Chem. Res. 44, 957−968.

Ryoo, S.R., Lee, J., Yeo, J., Na, H.K., Kim, Y.K., Jang, H., Lee, J.H., Han, S.W., Lee, Y., Kim, V.N., Min, D.H., 2013. ACS Nano 7, 5882−5891.

Sawyers, C.L., 2008. Nature 452, 548−552.

Shi, H.W., Zhao, W., Liu, Z., Liu, X.C., Xu, J.J., Chen, H.Y., 2016. Anal. Chem. 88, 8795−8801.

Wang, C., Lin, W., 2011. J. Am. Chem. Soc. 133, 4232–4235.

Wu, L., Hu, Y.F., Sha, Y.H., Li, W.R., Yan, T.T., Wang, S., Li, X., Guo, Z.Y., Zhou, J., Su, X.R., 2016. Talanta 160, 247–255.

Xiong, C., Wang, H., Liang, W., Yuan, Y., Yuan, R., Chai, Y.Q., 2015. Chem. Eur. J. 21, 9825–9832.

Yang, C., Dou, B., Shi, K., Chai, Y.Q., Xiang, Y., Yuan, R., 2014. Anal. Chem. 86, 11913–11918.

Yuan, Y.H., Wu, Y.D., Chi, B.Z., Wen, S.H., Liang, R.P., Qiu, J.D., 2017. Biosens. Bioelectron. 97, 325−331.

Yue, S.Z., Zhao, T.T., Bi, S., Zhang, Z.P., 2017. Biosens. Bioelectron. 98, 234–239.

Zhang, S.Q., Li, L.N., Zhao, S.G., Sun, Z.H., Luo, J.H., 2015. Inorg. Chem. 54, 8375−8379.

Zhou, W., Tian, Y.F., Yin, B.C., Ye, B.C., 2017. Anal. Chem. 89, 6120−6128.

Fig 1. TEM images of (A) g-C_3N_4, (B) g-C_3N_4@AuNPs, (C) Ru-MOF nanosheets, (D) Fe_3O_4@AuNPs, (E) Fe_3O_4@AuNPs-HP1-miRNA-141-sDNA1-AuNPs@g-C_3N_4 and (F) Fe_3O_4@AuNPs-HP2-miRNA-21-sDNA2-Ru-MOF.

Fig 2. (A) CV and (B) EIS curves for the stepwise biosensor fabrication measured in 0.1 M KCl containing 5.0 mM $[Fe(CN)_6]^{3-/4-}$ within the potential scan range of −0.2-0.6 V at the scan rate of 100 mV/s. (a) bare MGCE, (b) (a) + capture unit, (c) (b) + miRNA-141 and miRNA-21, and (d) (c) + signal unit 1 and signal unit 2. (C) CV responses of the prepared biosensor with or without g-C_3N_4@AuNPs and Ru-MOF nanosheets in 0.1 M PBS (pH 7.4) containing 20 mM $K_2S_2O_8$ and 60 mM TPrA. (D) ECL signals obtained from the differently modified electrodes in 0.1 M PBS (pH 7.4) containing 20 mM $K_2S_2O_8$ and 60 mM TprA. (a) bare MGCE, (b) (a) + capture unit, (c) (b) + miRNA-141 and miRNA-21, and (d) (c) + signal unit 1 and signal unit 2.

Fig 3. (A) ECL intensity from the biosensor in the presence of miRNA-141 and miRNA-21 at different concentrations of (a) 0.5, (b) 1, (c) 5, (d) 10, (e) 50, (f) 100, (g) 500, (h) 1000, (i) 5000 and (j) 10000 (fM). (B) Calibration curve obtained through plotting ECL intensity against the logarithmic concentrations of miRNA-141 (fM). (C) Calibration curve obtained through plotting ECL intensity against the logarithmic concentrations of miRNA-21 (fM).

Fig 4. (A) ECL emission from the biosensor in 0.1 M PBS (pH 7.4) containing 20 mM $K_2S_2O_8$ and 60 mM TPrA under continuous 8 cycles; (B) The specificity of the proposed ECL biosensor: blank, miRNA-101 (100 pM), miRNA-122 (100 pM),

miRNA-155 (100 pM), target of miRNA-141 (10 fM) and miRNA-21 (10 fM) solely, and the mixture containing miRNA-141 (10 fM) and miRNA-21 (10 fM).

Scheme 1. Schematic diagram of the preparation procedure of (A) signal unit 1 (g-C_3N_4@AuNPs-sDNA1), (B) signal unit 2 (Ru-MOF-sDNA2), and (C) the proposed potential-resolved Faraday cage-type ECL biosensor for the determination of dual targets miRNA-141 and miRNA-21.

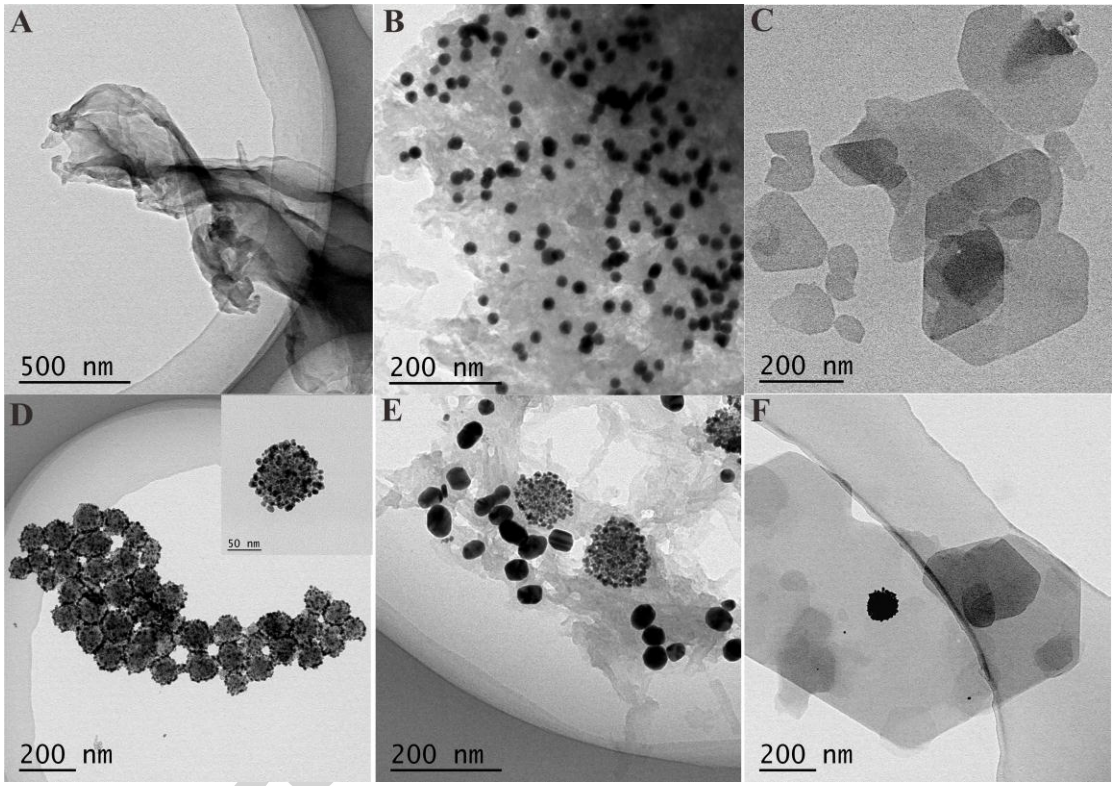

Fig. 1

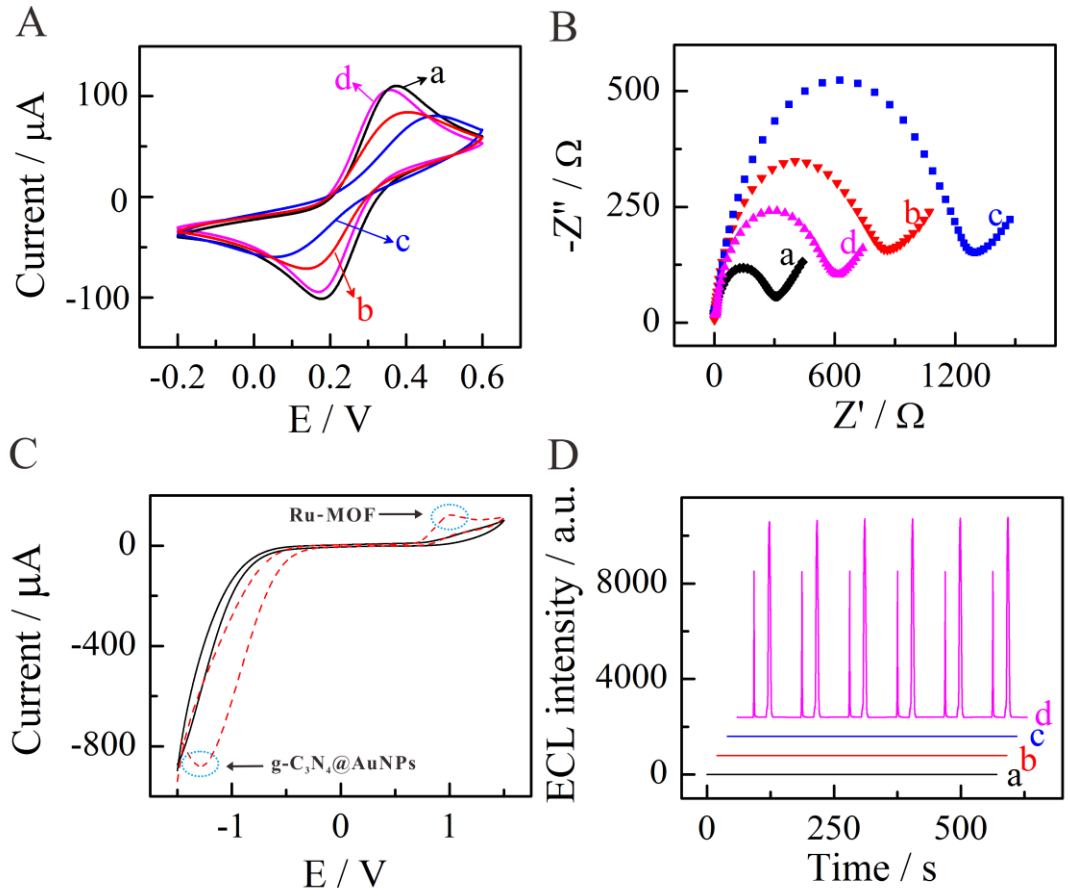
A
Current / μA
E / V
a
b
c
d
B
-Z'' / Ω
Z' / Ω
C
Current / μA
E / V
Ru-MOF
g-C3N4@AuNPs
D
ECL intensity / a.u.
Time / s
a
b
c
d

Fig. 2

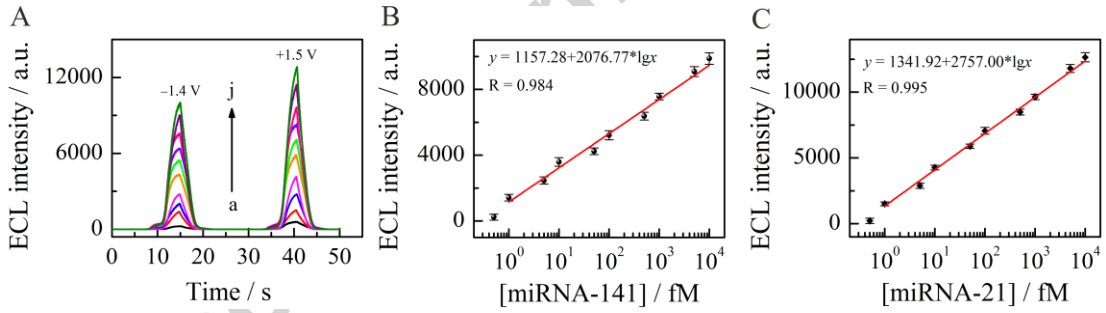
A
ECL intensity / a.u.
Time / s
-1.4 V
+1.5 V
j
a
B
ECL intensity / a.u.
y = 1157.28+2076.77*lgx
R = 0.984
[miRNA-141] / fM
C
ECL intensity / a.u.
y = 1341.92+2757.00*lgx
R = 0.995
[miRNA-21] / fM

Fig. 3

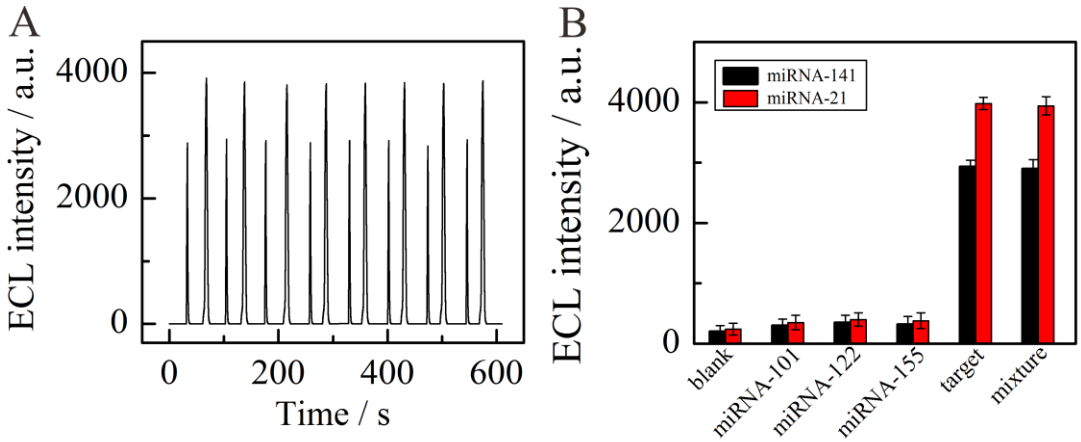

Fig. 4

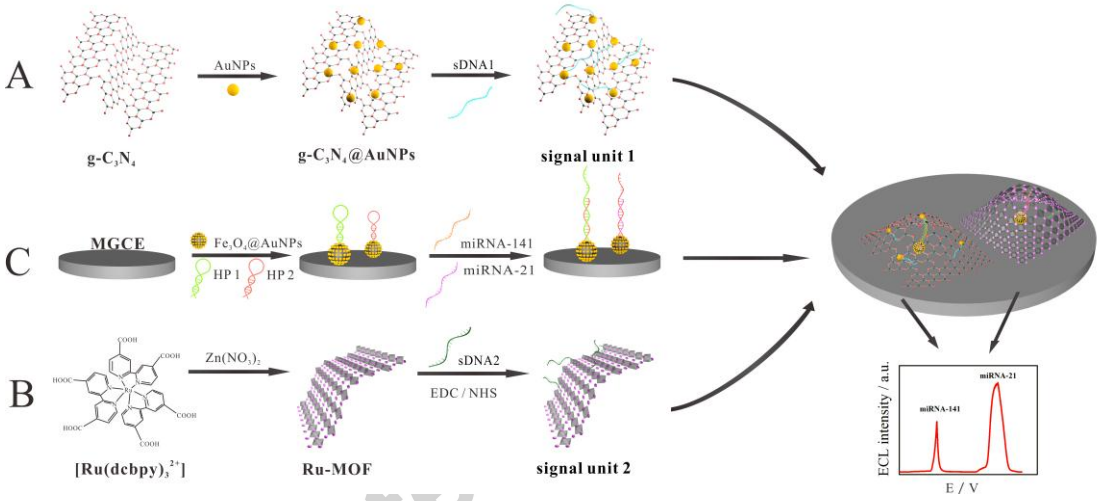

Scheme

Table 1 Recovery tests for miRNA-141 and miRNA-21 in spiked human serum samples ($\bar{x} \pm s$, n = 3).

Samples		Added (fM)	Found (fM)	RSD (%)	Recovery (%)
1	miRNA-141	5.0	5.4 ± 0.4	7.4	108.0
	miRNA-21	5.0	4.6 ± 0.4	8.7	92.0
2	miRNA-141	50.0	53.7 ± 2.8	5.2	107.4
	miRNA-21	50.0	54.8 ± 3.6	6.6	109.6
3	miRNA-141	500.0	465.7 ± 19.1	4.1	93.1
	miRNA-21	500.0	528.4 ± 22.7	4.3	105.7

Highlights

- OHP-extended potential-resolved Faraday cage-type ECL biosensor was developed.
- Two ECL probes of g-C_3N_4@AuNPs and Ru-MOF nanosheets for miRNAs detection were prepared.
- A new biosensor for simultaneous detection of miRNA-141 and miRNA-21 was obtained.
- This strategy offers a new method and perspective for miRNAs detection.